Comparative Study on the Effects of Noise in ML-Based Anxiety Detection

Schapiro, S.; Alkurdi, A., Hsiao-Wecksler, E.

———————————— ✦ ————————————

CONTENTS

1   ABSTRACT

Wearable health devices are ushering in a new age of continuous and noninvasive remote monitoring. One application of this technology is in anxiety detection. Many advancements in anxiety detection have happened in controlled lab settings, but noise prevents these advancements from generalizing to real-world conditions. We seek to progress the field by studying how noise impacts model performance and developing models that are robust to noisy, real-world conditions and, hence, attuned to the commotion of everyday life. In this study we look to investigate why and how previous methods have failed. Using the wearable stress and affect detection (WESAD) dataset, we compare the effect of various intensities of noise on machine learning models classifying levels of physiological arousal in the three-class classification problem: *baseline vs. stress vs. amusement*. Before introducing noise, our baseline model performance reaches 98.7%, compared to Schmidt 2018's 80.3%. We discuss potential sources of this discrepancy in results through a careful evaluation of feature extraction and model architecture choices. Finally, after the introduction of noise, we provide a thorough analysis of the effect of noise on each model architecture.

2   INTRODUCTION

The proliferation of remote wearables like the Apple Watch, Dexcom Continuous Glucose Monitor, and AliveCor Kardia into consumer markets marks a new age of continuous and noninvasive health monitoring. Affordable consumer electronics like these can now read heart rhythms, monitor blood oxygen levels, measure blood glucose, and gauge electrodermal activity very accurately at any place or time. One application of this technology is in anxiety detection.

Anxiety is triggered by a sympathetic nervous system response that releases compounds like cortisol and adrenaline into the bloodstream, causing an increase in heart rate, temperature, breathing rate, and muscular tension in preparation for a physical response. Chronic anxiety and stress are associated with a number of health risks, such as headaches, insomnia, and increased risk of cardiovascular disease[1]. Consequently, developing a remote monitoring solution to notify patients when anxiety levels are elevated can allow them to calm themselves and mitigate these health risks.

One complication associated with remote monitoring is noise. The commotion and movement of everyday life can obfuscate signals, making it difficult for remote monitors to perform as well as laboratory equipment. Thus, the purpose of this study is to introduce various intensities of noise to signals obtained in a controlled environment and evaluate the resistance of anxiety classification models to this noise.

3   METHODS

We start our investigation by introducing noise to an existing dataset, allowing us to compare our findings with previous bodies of work.

3.1   Data

This study required a dataset containing physiological readings concurrent with labeled levels of physiological arousal. An open-source dataset called wearable stress and affect detection (WESAD) contains both of these and is composed of a collection of physiological and motion signals sampled from 15 participants exposed to stimuli eliciting three levels of arousal—*baseline*, *amusement*, and *stress*—while electrocardiogram (ECG), electrodermal activity (EDA), electromyograph (EMG), respiration (RESP), temperature (TEMP), blood volume pulse (BVP), and accelerometer (ACC) readings were sampled from the chest and wrist. A RespiBAN
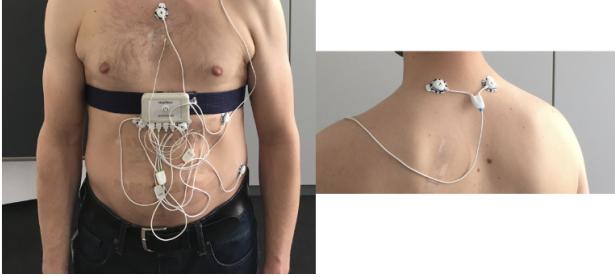
Fig. 1. Placement of the RespiBAN and ECG, EDA, EMG, TEMP sensors[1].

Professional was used to sample chest data, and an Empatica E4 was used to sample wrist data[1] (see *Figure 1*). These 15 participants were exposed to stress-eliciting stimuli for 10 minutes through a Trier Social Stress Test, amusement-eliciting stimuli for 6 minutes by watching funny videos, and a baseline level of stimuli for 20 minutes. In between stimuli, participants were instructed to meditate to return back to a baseline state. The total duration of sampling for each participant was approximately two hours[1]. In conclusion, the WESAD dataset contains physiological and motion signals synchronized with levels of arousal-eliciting stimuli, the former of which can be used to predict the latter in a machine learning (ML) classification problem.

3.2 Noise Artifact

Our comparative study starts by introducing various levels of noise to physiological signals. To do this, we must quantify how we are measuring the intensity of noise. Given a signal S, we define the signal to noise ratio, SNR, as

$$ SNR = \frac{\mathbb{E}[S^2]}{\mathbb{E}[N^2]}, \tag{1} $$

where $\mathbb{E}[\cdot]$ denotes the expected value and assumes the form $\mathbb{E}[X] = \int_{-\infty}^{\infty} x p(x) dx$ for a continuous random variable X with probability density function $p(x)$. $\mathbb{E}[S^2]$ and $\mathbb{E}[N^2]$ are defined as the *power* of the signal and noise, respectively. Consequently, SNR is a comparison between the signal's power and the noise's power. In this study, we tested 10 signal to noise ratios, evaluating various intensities of noise artifact on classification accuracy. We initially tested five benchmark SNRs (0.1, 0.2, 0.3, 0.4, 0.5), and thoughtfully chose the remaining five (0.001, 0.01, 0.05, 0.15, 0.6) after examining performance plots in *Figure 3*. In conclusion, we tested the following SNRs:

$$ \{0.001, 0.01, 0.05, 0.1, 0.15, 0.2, 0.3, 0.4, 0.5, 0.6\}. \tag{2} $$

3.2.1 Gaussian Noise

For the first stage of this study, we chose to introduce Gaussian noise. While there are other choices of noise, many of which we plan to test in the future, because noise is often the aggregate of many environmental perturbations, and the central limit theorem holds that the sum of N independent random variables tends towards a Gaussian distribution for large N, this made Gaussian noise the most compelling and comprehensive choice of noise for the first stage of the study.

We used non-additive Gaussian noise so that the mean μ of the Gaussian distribution we sampled from was 0. Our noise was also time-invariant, in that the distribution we sampled from at every time step of the signal did not change. These choices were made to simplify the structure of the noise and provide a baseline against which we could later compare more complex forms of noise. As will be discussed in the conclusion, extensions of this study should introduce *additive* and/or *time-variant* Gaussian noise, among other choices.

For non-additive, time-invariant Gaussian noise $N(\mu, \sigma^2)$, recall from the definition of variance that $Var[N] = \mathbb{E}[N^2] - \mathbb{E}^2[N]$, so that $\mathbb{E}[N^2] = Var[N] + \mathbb{E}^2[N] = \sigma^2 + \mu^2$. Since we set $\mu = 0$ to make the noise non-additive, $\mathbb{E}[N^2]$ is simply equivalent to σ^2. Then, recall from equation **(1)** the definition of SNR, which implies that

$$ \sigma^2 = \mathbb{E}[N^2] = \frac{\mathbb{E}[S^2]}{SNR} \tag{3} $$

For a given signal S, the power of the signal $\mathbb{E}[S^2]$ is computed by squaring each value of the signal to create S_{sq} and then taking the average of S_{sq}, so that

$$ \mathbb{E}[S^2] = \frac{1}{L} \sum_{i=1}^{L} S_{sq,i}, \tag{4} $$

where L is the length of the signal S_{sq}. We then construct a Gaussian probability density function of the form

$$ f(x) = \frac{1}{\sigma\sqrt{2\pi}} \exp\left(\frac{-x^2}{2\sigma^2}\right), \qquad \text{where} \tag{5} $$

$$ \sigma = \frac{\mathbb{E}[S^2]}{SNR} \qquad \text{and} \tag{6} $$

$$ \mathbb{E}[S^2] = \frac{1}{L} \sum_{i=1}^{L} S_{sq,i} \tag{7} $$

and sample from that. For each of the 15 subjects in the WESAD data, equation **(5)** is repeated for each signal across both wrist and chest sensor modalities. A noised set of signals for each subject is then created. The original, clean signals for each subject are later used as a baseline to compare against the noised signals we construct. In total, for each of the 15 patients, 11 sets of signals at various noise levels—ranging from a clean signal to an SNR of 0.001—are used in feature extraction and modeling. *Figure 2* shows an example of a noised ECG signal for one patient.

3.3 Feature Extraction

Feature extraction is then done for each of the 15 patients and their 11 sets of signals in an iterative process. The following explanation will outline how feature extraction is done for one set of signals, and the exact same logic can be applied to any other set of signals, noisy or clean.

We start by segmenting the signal into windows of 30 seconds, a length used in Healey 2005[3]. A window shift of 30 seconds is also used, which eliminates any overlap between successive windows. Next steps of this study will evaluate the impact of additional window lengths and stride sizes on performance.
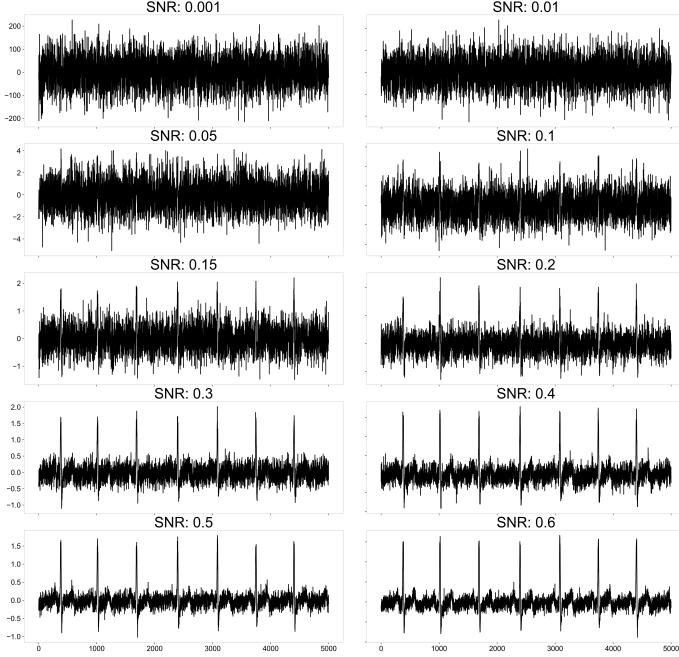
Fig. 2. ECGs after the introduction of noise.

A butter lowpass filter, available through the *scisig* library is applied to the EDA on the chest and wrist. We use the *heartpy* library to compute ECG features, the *neurokit2* library to compute the skin conductance level (SCL) and skin conductance response (SCR) of the EDA, the *biosppy* library to compute RESP features, and the *scisig* library again to compute peak frequency. Other features are computed using *numpy* and *pandas*.

In the end, after feature extraction is done for each patient and concatenated together, there are 1179 total observations of 118 features paired with a label (1 for *baseline*, 2 for *stress*, and 0 for *amusement*). The name and description of each feature we compute is shown in TABLE 1. Each feature is computed on both the Respiban Professional chest data and the Empatica E4 wrist data.

3.4 Models

The aforementioned extracted features are passed as inputs into five ML models:

- Linear Discriminant Analysis (LDA),
- Support Vector Machine (SVM),
- Random Forest (RF),
- ADABoost (ADA),
- and XGBoost (XGB).

LDA, RF, and ADA were chosen to compare our results with those achieved in Schmidt 2018. SVM, although an outdated classification algorithm by this point, was chosen to allow comparisons between our work and historical studies[4,5,6]. Finally, XGB was chosen because its scalable gradient boosting architecture makes it equipped to handle large, complex datasets with great efficiency and accuracy[2].

Before feature data is passed into these models, we use a standard scaler. This normalizes each feature, such that for each feature f, we compute

$$f^* = \frac{f - \text{mean}(f)}{\text{std}(f)} \tag{8}$$

and use f^* instead of f when modeling. Normalization is done so that each feature has unit standard deviation and the same mean of 0. Otherwise, some features with naturally larger variance or mean might arbitrarily dominate model performance, leading to an avoidable degradation in accuracy. For ADA, XGB, and RF, the number of base estimators was set to 100. For the SVM, we used a linear kernel and a C parameter of 1. This C value is inversely proportional to the strength of the regularization. The *sklearn* library is used for LDA, SVM, RF, and ADA, while the *xgboost* library is used for XGB. Classification accuracy, which we will hereafter refer to simply as accuracy, is calculated as

$$\frac{TP + TN}{TP + TN + FN + FP} \tag{9}$$

where TP is the number of true positives, TN, is the number of true negatives, FN is the number of false negatives, and FP is the number of false positives. This is the conventional method of calculating accuracy and was used in the Schmidt 2018[1] and Healey 2005[3] studies, allowing a comparison between our work and theirs.

4 DISCUSSION

4.1 Results Without Noise

We first test on the clean dataset to attain a benchmark accuracy we compare with the noised datasets. TABLE 2 contains the accuracies, as calculated in equation **(7)**, achieved by each model. The results are generally consistent with our expectations, with RF and XGB, the two tree based models, performing the best. XGB achieves the highest accuracy, which is expected due to the model's ability to capture complexity and non-linearity within data[2]. ADA performs poorly despite having the same number of base estimators as the XGB model.

We now look to feature importance as context to better interpret these results. To start, we examine the pearson correlation coefficient between each feature f and the level of arousal a. The 10 features with the highest pearson correlation coefficients to the level of arousal are shown in TABLE 3. The pearson correlation coefficient between a feature f and the level of arousal a is computed in the following way

$$\frac{\sum_{i=1}^{N}(f_i - \mu_f)\sum_{i=1}^{N}(a_i - \mu_a)}{\sqrt{\sum_{i=1}^{N}(f_i - \mu_f)^2 \sum_{i=1}^{N}(a_i - \mu_a)^2}}, \tag{10}$$

where N is the number of observations (1179 in this case), μ_f is the mean of the feature, and μ_a is the mean of the arousal level. This measure captures the tendency for two variables, f and a in this case, to be above or below their mean at the same time and by how much.

We also look at mean decrease in impurity (MDI) of a single decision tree as a measure of feature importance. MDI is computed according to Gini importance, which reflects

Signal	Feature	Description
ACC	$\mu_{ACC,i}, \sigma_{ACC,i} \quad i \in \{x,y,z,3D\}$ $\min_{ACC,i}, \max_{ACC,i} \quad i \in \{x,y,z,3D\}$ $\| \int_{ACC,i} \| \quad i \in \{x,y,z,3D\}$ $f_{ACC,j}^{peak} \quad j \in \{x,y,z\}$	Mean, std. dev. for each axis separately and summed over all axes Min, max for each axis separately and summed over all axes Absolute integral for each axis Peak frequency for each axis i
EDA	$\mu_{EDA,i}, \sigma_{EDA,i} \quad i \in \{EDA, SCR, SCL\}$ $\min_{EDA,i}, \max_{EDA,i} \quad i \in \{EDA, SCR, SCL\}$ $\partial_{EDA,i}, \text{range}_{EDA,i} \quad i \in \{EDA, SCR, SCL\}$	Mean, std. dev. for each component of the EDA Min, max of each component of the EDA Slope and dynamic range of each component of the EDA
TEMP	$\mu_{TEMP}, \sigma_{TEMP}$ $\min_{TEMP}, \max_{TEMP}$ $\partial_{TEMP}, \text{range}_{TEMP}$	Mean, std. dev. of the TEMP signal Min, max of the TEMP signal Slope and dynamic range of TEMP signal
RESP	$\mu_{RESP,i}, \sigma_{RESP,i} \quad i \in \{Inhale, Exhale\}$ $\min_{RESP,i}, \max_{RESP,i} \quad i \in \{Inhale, Exhale\}$ I/E rate_{RESP}	Mean, std. dev. of RESP signal for inhale and exhale Min, max of RESP Signal for inhale and exhale Inhale/exhale ratio Breath rate
EMG	μ_{EMG}, σ_{EMG} $\min_{EMG}, \max_{EMG}$ $\| \int_{EMG} \|$ range_{EMG}	Mean, std. dev. of the EMG signal Min, max of the EMG signal Absolute integral of the EMG signal Dynamic range of the EMG signal
ECG	$NN50, pNN50$ BPM IBI $\min_{ECG}, \max_{ECG}$ μ_{ECG}, σ_{ECG} $SDSD, RMSDD$ $SDNN$	Number and percentage of NN intervals differing more than 50ms Heartbeats per minute Interbeat interval Min, max of the ECG signal Mean, std. dev. of the ECG signal Std. dev. and root mean square of successive differences Std. dev. of NN intervals
BVP	μ_{BVP}, σ_{BVP} $\min_{BVP}, \max_{BVP}$ f_{BVP}^{peak}	Mean, std. dev. of the BVP signal Min, max of the BVP signal Peak frequency of the BVP signal

TABLE 1
Extracted features.

Model	Accuracy
LDA	0.9322
SVM	0.9449
RF	0.983
ADA	0.7712
XGB	**0.987**

TABLE 2
Baseline model accuracies.

the reduction of the Gini criterion brought by the feature under consideration[1]. The features with the top 10 largest MDI are shown in TABLE 4.

The correlation analysis shows an importance heavily dominated by the EDA and ECG, and the MDI corroborates this finding with the EDA and ECG features also contributing significantly to MDI. These results are quite different from those attained in Schmidt 2018[1], which saw the std. dev. of chest RESP, the mean heart rate of the chest ECG,

Feature	Correlation
$\max_{EDA,SCL}^{wrist}$	0.6457
$\mu_{EDA,SCL}^{wrist}$	0.6401
$\min_{EDA,SCL}^{wrist}$	0.6332
BPM^{chest}	0.5359
$\max_{EDA,SCL}^{chest}$	0.5182
IBI^{chest}	0.5155
$\mu_{EDA,SCL}^{chest}$	0.5132
$\min_{EDA,SCL}^{chest}$	0.5076
$\sigma_{EDA,SCR}^{wrist}$	0.4185
$\sigma_{EDA,SCR}^{chest}$	0.4162

TABLE 3
Top 10 highest correlation features without noise.

Feature	MDI
$\mu_{EDA,SCL}^{chest}$	0.0879
$\min_{EDA,SCL}^{chest}$	0.0853
$\max_{EDA,SCL}^{chest}$	0.0716
$\mu_{EDA,SCL}^{wrist}$	0.0626
$\max_{EDA,SCL}^{wrist}$	0.0613
$\max_{EDA,SCL}^{wrist}$	0.0464
$\max_{EDA,SCR}^{wrist}$	0.0257
IBI^{chest}	0.0239
BPM^{chest}	0.0230
$\sigma_{EDA,SCR}^{wrist}$	0.0210

TABLE 4
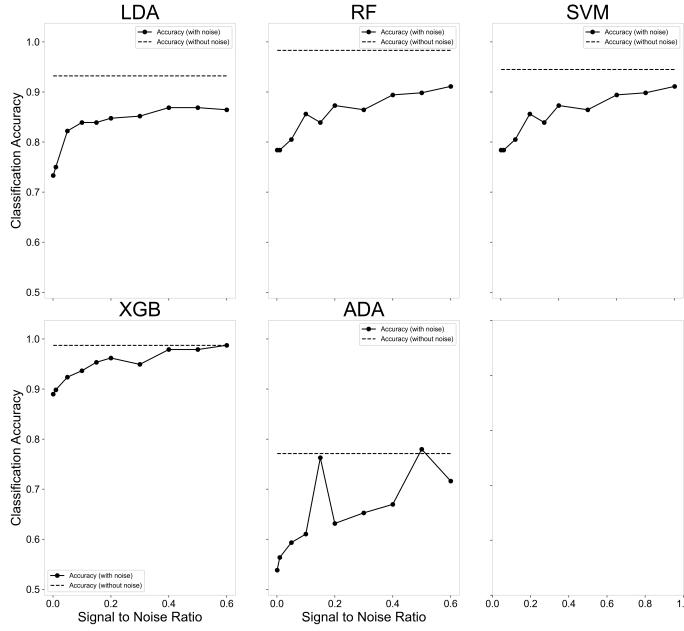Top 10 largest MDI features without noise.

Fig. 3. Model accuracy at each SNR.

the minimum wrist TEMP, the mean chest ACC, and wrist EDA dynamic range dominate its feature importance for the same classification task.

This may have occurred because we used a window size of 30 seconds and Schmidt 2018 used a window size of 60 seconds, because our features differed slightly in their calculation, or due to other discrepancies in data pre-processing. Understanding the cause of dichotomies between our work and historical studies will be the subject of future investigation.

4.2 Results With Noise

After introducing noise, we see an expected degradation in classification accuracy. *Figure 3* depicts the model accuracy of each of the five models for each SNR we tested. The dotted, horizontal line in each subplot represents the baseline accuracy we achieved before introducing noise, as shown in TABLE 2. Notice that in all of the plots the model accuracy increases asymptotically towards the baseline accuracy as the SNR increases.

We observe that the XGB architecture is most resistant to noise, achieving 90% accuracy even at a SNR of 0.001, where most signals have been entirely obfuscated. XGB also nearly reaches its baseline accuracy once a SNR of 0.4 is reached, whereas other models like the LDA, RF, and SVM still sharply differ from baseline performance at this level. We again look to feature importance at each SNR to better interpret these results. The top 10 features with the highest correlation to arousal levels at each SNR and their pearson correlation coefficients, calculated the same way as in **(7)**, are shown in TABLE 5, where the feature with the highest correlation at each SNR is bolded.

The EDA continues to dominate the correlation analysis, and we note the absence of any ECG feature from this table, indicating that the noise likely disrupted *heartpy*'s peak finding algorithm and rendered features like IBI and BPM uninformative.

Once again, we compute MDI to corroborate these findings. TABLE 6 shows the 10 features with the largest MDI at each SNR, with the feature having the largest MDI at each SNR in bold.

MDI tells a different story, largely being dominated by ACC features for lower SNRs. However, as the SNR increases to 0.3 and higher, we observe that the EDA plays an increasingly important role in classification accuracy. Understanding why the ACC data leads to the largest MDI at lower SNRs remains the subject of future investigation.

5 CONCLUSION

5.1 Summary

In this study we examined the effects of noise in feature-based anxiety detection with various ML architectures. Using the open-source WESAD repository—a dataset containing ECG, EDA, EMG, RESP, TEMP, BVP, and ACC physiological readings concurrent with labeled levels of physiological arousal—we set up an ML task to classify levels of physiological arousal from features of physiological signals. We then introduced various intensities of Gaussian noise to the physiological signals and examined how noise impacted classification accuracy for the LDA, SVM, RF, ADA, and XGB models. Our baseline performance achieved accuracies up to 98.7%, outperforming previous studies, and we observed that XGB was the most resilient model architecture after the introduction of noise, with somewhat conflicting feature importance data across the correlation and MDI analysis.

5.2 Next Steps

Further work will test additional SNRs and noise distributions. Distributions we believe are immediate extensions to the work presented here are:

- time-variant non-additive Gaussian noise,
- time-variant additive Gaussian noise,
- time-variant frequency domain noise,
- time-invariant frequency domain noise, and
- psuedo-realistic, which can be done by creating a function that maps ACC data to the magnitude of noise, and then excludes ACC data when modeling.

We will also evaluate various window sizes and stride lengths in the feature extraction process, which we believe contributed to the discrepancy between our results and those achieved in Schmidt 2018[1]. We also seek to continue developing a richer feature set.

Finally, subsequent studies can go into greater depth on the hyperparameter optimization process in model fitting, as well as include other classification algorithms like logistic regression, naive bayes, and k-nearest neighbors to expand comparability with other historical studies and potentially discover more noise resistant model variants. Along the way, a deeper investigation into feature importance will be done to better interpret the conflicting results we have found in this study.

Feature	SNR									
	0.001	0.01	0.05	0.1	0.15	0.2	0.3	0.4	0.5	0.6
$\mu^{wrist}_{EDA,SCL}$	-	-	-	0.361	0.403	0.475	**0.521**	**0.535**	0.546	**0.546**
$\max^{wrist}_{EDA,SCL}$	-	-	-	0.331	0.352	0.446	0.505	0.528	**0.547**	0.546
$\min^{wrist}_{EDA,SCL}$	-	-	-	0.339	0.371	0.449	0.503	0.514	0.534	0.536
$\max^{chest}_{EDA,SCL}$	**0.518**	**0.518**	**0.518**	**0.518**	**0.518**	**0.518**	0.518	0.518	0.518	0.518
$\mu^{chest}_{EDA,SCL}$	0.513	0.513	0.513	0.513	0.513	0.513	0.513	0.513	0.513	0.513
$\min^{chest}_{EDA,SCL}$	0.508	0.508	0.508	0.508	0.508	0.508	0.508	0.508	0.508	0.508
$\sigma^{chest}_{EDA,SCR}$	0.408	0.408	0.408	0.408	0.408	0.408	0.408	0.408	0.408	0.408
$\max^{chest}_{EDA,SCR}$	0.367	0.367	0.367	0.367	0.367	0.367	0.367	0.367	0.367	0.367
$\text{range}^{chest}_{EDA}$	0.320	0.320	0.320	0.320	0.320	0.320	0.320	0.320	0.320	0.320
$\mu^{chest}_{RESP,exhale}$	-	-	-	-	-	-	-	-	-	0.316
σ^{chest}_{EDA}	0.308	0.308	0.308	0.308	0.308	0.308	0.308	0.308	0.308	-
$\min^{chest}_{EDA,SCR}$	0.272	0.272	0.272	-	-	-	-	-	-	-
$\sigma^{chest}_{EDA,SCL}$	0.252	0.252	0.252	-	-	-	-	-	-	-
$\max^{chest}_{EDA}$	0.197	0.197	0.197	-	-	-	-	-	-	-

TABLE 5
Top 10 highest correlation features at each SNR.

Feature	SNR									
	0.001	0.01	0.05	0.1	0.15	0.2	0.3	0.4	0.5	0.6
$\min^{chest}_{ACC,z}$	0.100	0.113	0.107	0.101	0.094	0.093	0.082	0.082	0.088	0.092
$\mu^{chest}_{ACC,z}$	0.105	0.115	0.098	0.091	0.095	0.100	0.100	0.099	0.102	0.100
$\sigma^{chest}_{ACC,y}$	0.105	0.105	0.102	0.089	0.085	0.069	0.078	0.076	0.081	0.077
$\max^{chest}_{ACC,z}$	**0.171**	**0.158**	**0.165**	**0.179**	**0.171**	**0.156**	**0.146**	**0.150**	**0.145**	**0.143**
$\sigma^{chest}_{ACC,z}$	0.023	0.028	0.025	-	-	0.021	-	-	-	-
$\max^{chest}_{ACC,x}$	0.029	0.021	0.022	-	0.019	-	-	-	-	-
$\sigma^{chest}_{ACC,x}$	0.030	0.027	0.023	0.025	0.033	-	0.021	0.027	0.024	0.025
∂^{wrist}_{TEMP}	0.036	0.036	0.036	0.024	0.028	0.028	-	-	-	-
$\min^{chest}_{ACC,y}$	0.067	0.072	0.058	0.058	0.052	0.056	0.036	0.031	0.026	0.025
$\max^{chest}_{ACC,y}$	0.071	0.053	0.063	0.054	0.057	0.067	0.053	0.046	0.040	0.040
$\mu^{wrist}_{EDA,SCL}$	-	-	-	0.018	0.020	0.035	0.056	0.041	0.054	0.040
$\min^{wrist}_{EDA,SCL}$	-	-	-	-	-	-	0.027	0.031	0.028	0.034
$\max^{wrist}_{EDA,SCL}$	-	-	-	-	-	0.029	0.033	0.051	0.055	0.065

TABLE 6
Top 10 largest MDI features at each SNR.

6 REFERENCES

1) Philip Schmidt, Attila Reiss, Robert Duerichen, Claus Marberger, and Kristof Van Laerhoven. 2018. Introducing WESAD, a Multimodal Dataset for Wearable Stress and Affect Detection. In Proceedings of the 20th ACM International Conference on Multimodal Interaction (ICMI '18). Association for Computing Machinery, New York, NY, USA, 400–408. https://doi.org/10.1145/3242969.3242985

2) Chen, Tianqi; Guestrin, Carlos (2016). "XGBoost: A Scalable Tree Boosting System". In Krishnapuram, Balaji; Shah, Mohak; Smola, Alexander J.; Aggarwal, Charu C.; Shen, Dou; Rastogi, Rajeev (eds.). Proceedings of the 22nd ACM SIGKDD International Conference on Knowledge Discovery and Data Mining, San Francisco, CA, USA, August 13-17, 2016. ACM.

3) Healey, Jennifer and Rosalind W. Picard. "Detecting stress during real-world driving tasks using physiological sensors." IEEE Transactions on Intelligent Transportation Systems 6 (2005): 156-166.

4) Setz, C., Arnrich, B., Schumm, J., La Marca, R., Tröster, G., & Ehlert, U. (2010). Discriminating stress from cognitive load using a wearable EDA device. IEEE Transactions on information technology in biomedicine, 14(2), 410-417.

5) Liang, Y., Reyes, M. L., & Lee, J. D. (2007). Real-time detection of driver cognitive distraction using support vector machines. IEEE transactions on intelligent transportation systems, 8(2), 340-350.